circIGHG-Induced Epithelial-to-Mesenchymal Transition Promotes Oral Squamous Cell Carcinoma Progression via miR-142-5p/IGF2BP3 Signaling

Jingpeng Liu, Xiao Jiang, Ailing Zou, Zhaoyi Mai, Zhijie Huang, Liying Sun, and Jianjiang Zhao

ABSTRACT

Circular RNAs (circRNA) are a new member of endogenously produced noncoding RNAs that have been characterized as key regulators of gene expression in a variety of malignances. However, the role of circRNA in oral squamous cell carcinoma (OSCC) remains largely unknown. In this study, we identified unique circRNA that regulate OSCC progression and metastasis and pave roads for future research in early diagnosis, prevention, and treatment of OSCC. Transcriptomic analyses identified a circRNA derived from *IGHG* locus (*circIGHG*) as significantly upregulated in OSCC and positively associated with poor prognosis of OSCC. *circIGHG* directly bound *miR-142-5p* and consequently elevated IGF2BP3 activity. Knockdown of *circIGHG* led to impaired expression of IGF2BP3 and attenuated aggressiveness of OSCC cells. Epithelial–mesenchymal transition was the main mechanism through which *circIGHG*/IGF2BP3 promotes metastasis of OSCC. Overall, these results demonstrate that circIGHG plays a pivotal role in OSCC development and metastasis and has potential to serve as a biomarker and therapeutic target for early-stage diagnosis and treatment of OSCC.

Significance: These findings broaden our insights regarding regulation of OSCC progression by circular RNA and serve as a reference for future clinical research in OSCC diagnosis and treatment.

Introduction

Oral cancer is overall the eighth most common malignancy and the most prevalent disease in head and neck tumors, with 170,000 deaths and over 350,000 newly added cases in 2018 alone worldwide (1, 2). Squamous cell carcinoma accounts for over 95% of oral cancer, which is characterized by robust aggressiveness and frequent metastasis and recurrence (3). Although recent years have witnessed remarkable improvements in diagnosis and treatment, 5-year survival rate of patients with oral squamous cell carcinoma (OSCC) remains under 50% and lack of early detection is responsible for the high mortality (4, 5). Therefore, understanding the mechanisms of progression and metastasis of OSCC is an important goal in OSCC intervention.

Circular RNAs (circRNA) are a recently rediscovered type of endogenous noncoding RNA that are generated from backsplicing of precursor mRNAs and features distinguishable single-stranded, covalently closed loops, lacking 5′-3′ polarity (6, 7). Extensively distributed in cytoplasm, this unique structure makes circRNA more resistant to exonucleases and more stable than their linear RNA counterparts (8). For decades, circRNAs were nearly unexplored because of the facts that circRNA-specific backsplicing junction reads do not map to a linear reference genome and circRNAs do not have poly(A) tails and are therefore not detectable in most early RNA-sequencing datasets where poly(A)-enrichment is part of the library preparation protocol. Over the past few years, circRNAs have gained enormous investigations. Despite controversy and skepticism still hovering over circRNA research realm (9), there are increasing amount of studies showing that circRNAs have great potential as miRNA sponges in a complementary base-pairing manner, suppressing miRNA activity and thereby promoting translation and stability of downstream target genes (10). Such a circRNA/miRNA/mRNA signaling axis has been demonstrated to exert multiple functions in a broad variety of physiologic and pathologic conditions, particularly in cancers (11–13). Accumulating research has identified numerous noncoding RNAs that participate in OSCC progression regulation, including *miR-23a-3p*, which suppresses tumor growth in OSCC via targeting FGF2 (14), and *lncRNA-p23154*, whose inhibitory action over *miR-378a-3* facilitates GLUT1 expression, therefore promoting invasion and metastasis of OSCC (15). With a growing body of reports that indicate emerging roles and functions of circRNAs in OSCC, how circRNAs pathways delicately regulate OSCC progression still remains largely enigmatic and needs to be further explored.

Human immunoglobulin heavy chain G (*IGHG*) gene, located in chromosome region *14q32*, is known for polymorphism across populations and critically involved in immune response and human survival (16, 17). Although not quite often associated with cancers, dysregulation of *IGHG* was reported in multiple malignancies, including lung cancer, breast cancer, and gastric cancer (18–20). In this study, we identified a unique *IGHG*-derived circRNA, *hsa_circ_0000579* (termed *circIGHG*), whose upregulated expression was frequently observed in OSCC and associated with poor prognosis. Further investigations demonstrated that *circIGHG* facilitates epithelial–mesenchymal transition (EMT) by regulating IGF2BP3 via directly sponging *miR-142-5p*, thereby leading to increased aggressiveness of OSCC. Those findings endow *circIGHG* promising potentials in serving as a novel diagnostic and therapeutic marker in OSCC.

Department of Oral Surgery, Stomatological Hospital, Southern Medical University, Guangzhou, Guangdong, China.

Note: Supplementary data for this article are available at Cancer Research Online (http://cancerres.aacrjournals.org/).

Corresponding Author: Jianjiang Zhao, Stomatological Hospital, Southern Medical University, Guangzhou, Guangdong 510220, China. Phone: 86-020-84439500; E-mail: zjj2521@sina.com

Cancer Res 2021;81:344–55

doi: 10.1158/0008-5472.CAN-20-0554

Materials and Methods

RNA isolation, RNase R treatment, and PCR

Total RNA was isolated using RNAprep Pure kits (DP430, DP431, Tiangen) according to the manufacturer's guidelines from either liquid nitrogen–frozen tissues or cultured cells. Concentration and purity for each RNA extract was checked by 260/280 ratio on a NanoDrop 2000 instrument (Thermo Fisher Scientific) using RNA-specific protocol. First-strand cDNA synthesis was achieved by using FastKing RT Kit (KR116, Tiangen). Quantitative PCR was performed with the Talent qPCR premix Kit (FP209, Tiangen) following the product's instructions. Primers used in this study were designed using Primer Bank (https://pga.mgh.harvard.edu/primerbank/) and Primer3Plus (V2.5.0). Primer sequences were listed in Supplementary File S1; Supplementary Table S1. Three technical replicates were set for each single reaction to ensure reliability and validity. Reactions were programmed for one cycle of denaturation for 1.5 minutes at 95°C, followed by 40 cycles of extension including 30 seconds at 95°C, 50 seconds at 57°C, and 1.5 minutes at 72°C. The $\Delta\Delta C_T$ value of the target genes' expression was measured and assessed against the value of the reference gene *GAPDH*.

RNase R treatment was performed by incubating 2 μg of total RNA mixture at 37°C for 10 minutes, as suggested by the product's manual (RNR07250, Lucigen). Following removal of linear forms, qRT-PCR qualification was performed to confirm the circular structure of *circIGHG*. Sanger sequencing covering the backsplicing junction sequence was performed using the qRT-PCR product of *circIGHG* (Geneseed). A total of 1% agarose gel was used for DNA electrophoresis.

RNA FISH

RNA FISH was performed using the Fluorescent *in situ* Hybridization Kit (C10910, RiboBio) according to the manufacturer's instructions. Cy3-labeled probes targeting *circIGHG* and Dig-labeled *miR-142-5p* probes (see Supplementary File S1, Supplementary Table S2) were synthesized by RiboBio Technology Co. Ltd. Fluorescence was excited and recorded with a Zeiss confocal laser scanning microscope (LSM 880 with Airyscan, Carl Zeiss).

RNA pull-down assay

RNA pull-down assay was performed referring to *Lal A*'s introduction (21). Biotinylated *circIGHG* and *miR-142-5p* probes were synthesized and transfected into CAL-27 cells, according to the manufacturer's protocol (RiboBio). Twenty-four hours later, cells were lysed and centrifugated to collect cytoplasmic contents, which were then incubated with C-1 magnetic beads (Life Technology) at 4°C for 5 hours. Pull-down RNA released from the beads after cleansing were evaluated by qRT-PCR.

RNA immunoprecipitation

RNA immunoprecipitation (RIP) experiments were performed with an EZ-Magna RNA Binding Protein Immunoprecipitation Kit (17-701, Millipore) according to the manufacturer's guidelines. Briefly, 2×10^7 human oral keratinocytes (HOK) and CAL-27 cells were collected and resuspended in 200 μL RIP lysis buffer. A total of 100 μL of each cell lysates were incubated with A/G magnetic beads conjugated with argonaute 2 (AGO2 antibody; NBP2-67121; Novus) or control protein of rabbit IgG with gentle agitation at 4 °C overnight. Immunoprecipitated RNA was then purified and measured by qRT-PCR for enrichment.

IHC and immunofluorescent staining

A total of 8-μm-thick serial formalin-fixed paraffin-embedded sections and frozen sections were used to serve IHC and immunofluorescent (IF) staining as described previously (22). Primary antibodies against Ki-67, IGF2BP3, E-cadherin, SNAI, ZEB2, and caspase-3 were used in this study (see Supplementary File S1; Supplementary Table S3). Sections were blocked with 10% normal goat serum at room temperature for 1 hour after deparaffinization and antigen retrieval, incubated with primary antibodies at 4°C overnight and horseradish peroxidase (HRP)-conjugated secondary antibodies at room temperature for 1 hour, and visualized with 3,3′-diaminobenzidine buffer in IHC. Secondary antibodies conjugated to Alex Fluor IgG were used for immunofluorescence. Nuclei were shaded with DAPI. All sections were examined and validated by two certified pathologists.

Western blotting

Protein extracts were isolated from OSCC cells using protein extraction kit (KGP250, KeyGene), and then electrophoresed through SDS-PAGE gels and transferred onto polyvinylidene difluoride membranes (Millipore) in equal amount, quantified BCA Protein Assay Kit (CW0014S, CWBIO), blocked with 0.5% BSA and incubated with primary antibodies at 4°C overnight. Membranes were then incubated with HRP-conjugated secondary antibodies, illuminated using chemiluminescence regents and visualized under a molecular imaging system (Bio-Rad).

Cell cultures and patient specimens

HOK and CAL-27 cells were purchased from Tongpai Technology. SSC-9, HSC-3, and HSC-6 cells were obtained from CinoAsia Co., Ltd. HOK cells were cultured in defined Keratinocyte SFM medium (10744019, Thermo Fisher Scientific). CAL-27, HSC-3, and HSC-6 cells were appropriately cultured in DMEM (SH30243.01, Hyclone) supplemented with 10% FBS and 0.5% penicillin-streptavidin solution according to the vendor's guidelines. SSC-9 cells were cultured in DME/F-12 medium (SH30023.01, Hyclone) supplemented with 10% FBS and 0.5% penicillin-streptavidin mixture. Cells were kept in a humidified incubator at 37°C with 5% CO_2. A total of 169 pairs of tumor and adjacent nontumor specimens were collected from clinically diagnosed patients with OSCC (97 males and 72 females, ages from 26 to 79 years old) in the Stomatological Hospital of Guangdong Province and immediately snap frozen in liquid nitrogen before undergoing further processing. Four pairs were deployed for circRNA microarray, which was performed on CapitalBio Technology Human CircRNA Array v2 chips (CapitalBio, Corp.) containing four identical arrays per slide. Each array possesses probes targeting 18×10^4 human circRNA sequences from CircBase, Deepbase, and Rybak-Wolf 2015. Ten pairs were used to solidify the microarray results. All 169 pairs served evaluating correlation between *circIGHG* and OSCC prognosis.

Cell proliferation assay

Cell counting kit-8 (CCK8) assay was done according to the manufacturer's protocol. Briefly, 5,000 cells were seeded into each unit in a 96-well palate and cultured in a humified chamber at 37°C for 24 hours before receiving treatment of 10 μL CCK8 solution for 2 hours. Absorbance were assessed at 450 nm on a microplate reader. Mean values from triplicates represent cell proliferative ability.

Apoptosis assay

Cells were induced to undergo apoptosis by addition of 10 μL 100 μmol/L carbonyl cyanide 3-chlorophenylhydrazone (CCCP) to the regular culturing medium for 20 minutes before being fixed by 4% paraformaldehyde. Relative intensity of caspase-3 expression was then checked to reflect apoptotic activity.

Lentivirus construction and transfection

siRNA oligos targeting *circIGHG* and IGF2BP3 were designed (Geneseed) and constructed into lentivirus (GenePharma), which were then transfected into CAL-27 cells. Stable transfection was established and maintained by culturing CAL-27 cells in regular medium supplemented with 0.2% puromycin. An upstream GFP tracer was also incorporated to indicate successful transfection. Exogenous truncated *circIGHG* containing sequences of both *miR-142-5p* binding sites and head-to-tail junction sequence was synthesized and introduced into CAL-27 cells to mimic the overexpression of *circIGHG* (Geneseed) as described before (23).

Northern blot analysis

circIGHG-specific probes (Supplementary File S1; Supplementary Table S2) were designed and synthesized by Zoonbio. *circRNA* was purified and enriched through RNase R treatment followed by polyadenylation and poly $(A)^+$ RNA depletion, electrophoresed in a 1% agarose gel with 6.7% formaldehyde and transferred to charged nitrocellulose membrane (Millipore), UV cross-linked and hybridized with Dig-labeled probes and radioactivated on an X-ray film. Analysis of *circIGHG* was performed in reference to an UltraRanger DNA ladder (NGB-12100, Norgen Biotek) that was Dig-coupled via a customized protocol (Telenbiotech).

Luciferase reporter assay

Similar luciferase reporter assay protocols were described in our previous report (24). Wild-type and binding site-specific mutated *circIGHG* and IGF2BP3–3′ untranslated region (UTR) sequences were synthesized and integrated into psiCHECK 2.0 vectors (Geneseed) and cotransfected into 293T cells with *miR-142-5p* mimics or *miR-142-5p* inhibitors, respectively, using lipofectamie 2000 reagent (Invitrogen). Cells were lysed and luciferase intensity was measured 48 hours after transfection. The ration of *Renilla* luciferase over firefly luciferase absorbance was calculated to quantitatively assess the interaction between *circIGHG* and *miR-142-5p*.

Animal experiments

All mice used in this study were housed and manipulated in the Central Laboratory of Southern Medical University in obedience with the institutional guidelines for animal use and care. Mice were accommodated for adaption for 1 week before being injected with cells either subcutaneously or into caudal veins. Subcutaneous xenograft tumor growth was monitored weekly in a live animal imaging instrument (Bruker). The excitation and emission wavelengths for GFP were 470 and 535 nm, respectively. Anesthesia was induced and maintained by 10% isoflurane during exposure. Subcutaneous and caudal vein injection was performed with 100 μL normal saline suspension of 10^6 cells using a 1 mL insulin syringe. Animals' weight was monitored weekly following injection. Euthanasia was initiated by CO_2 suffocation and finished by cervical dislocation. Xenograft tumors and lungs were collected following euthanasia.

Statistical analysis

circRNA microarray data were initially preprocessed by using Feature Extraction Software v10.7 (Agilent). Transcription differences and statistical significance *P* value were calculated using GeneSpring GX (Agilent). Bioinformatic prediction and circRNA-miRNA network was generated in miRanda (GeneCopoeia Inc.). Ordinary one-way ANOVA analysis (multiple comparisons were included when necessary) was performed in Graphpad Prism 7 (Graphpad Software) to compare protein expression differences among groups in Western blots and immunofluorescence assays. Means ± SD were presented in quantification bar graphs. Cox regression analyses were conducted in SPSS (V20.0, IBM). Mice's weight changes among groups were compared by *t* test.

Ethics approval and consent to participate

Ethics approval was issued by the Ethics Committee of Stomatological Hospital of Southern Medical University (Guangzhou, China).

Results

circIGHG is overexpressed in OSCC tissue and cells

To profile the significantly differentially expressed circRNAs in OSCC, circRNA microarray was performed on four pairs of OSCC and adjacent nontumor tissues. Overall, the assay revealed a total of 8,068 circRNAs, which were remarkably altered with |fold change| >2 and $P < 0.01$ in OSCC, including 5,012 upregulated and 3,056 downregulated (see the full list in Supplementary File S2), in comparison with nontumor tissue (**Fig. 1A**; Supplementary File S3; Supplementary Fig. S1). Multiple plotting analyses verified the varied expression (**Fig. 1B** and **C**).

Among those significantly dysregulated circRNAs, *circIGHG* (*hsa_circ_0000579*) stands out the pool as being upregulated by 109 folds in OSCC and more importantly, showing powerful "miRNA sponges" potential, as being ranked the top circRNAs with largest number of miRNA targets (see Supplementary File S3; Supplementary Fig. S2). *circIGHG* is transcribed from a hybrid region between the gene *IGHG1* and *IGHG3* (*IGHG3* exon 2–9 and *IGHG1* exon 1 and 2) on the minus strand of chromosome 14 in human genome, whose spliced sequence length is 27,944 bp (**Fig. 1D**; Supplementary File S4), confirmed by Northern blotting assay (Supplementary File S3; Supplementary Fig. S3). RNase R digestion resistance substantiated the existence of the circular form of *circIGHG* (**Fig. 1E**). Sanger sequencing further illustrated the sequence of the head-to-tail junction site (**Fig. 1F**). In addition, qRT-PCR assays exhibited remarkably higher *circIGHG* expression in both OSCC tissue samples (average fold change = 18.71, $P < 0.001$) and cell lines (average fold change = 10.67, $P < 0.001$) in OSCC than controls, which solidified the altered *circIGHG* expression (**Fig. 1G** and **H**). In particular, the most intensified *circIGHG* expression was steadily seen in CAL-27 cells (fold change = 20.95, $P < 0.001$), which was then chosen to carry out the following investigations. Those results strongly indicated that *circIGHG* was significantly upregulated in OSCC. Further studies therefore were demanded to explore how upregulated *circIGHG* mediates OSCC progression.

Overexpression of *circIGHG* was associated with poor prognosis in patients with OSCC

To study the significance of dysregulation of *circIGHG* from clinicopathologic perspective, we collected a total of 169 pairs of cancer and adjacent normal tissue from patients with clinically confirmed OSCC. Patients' detailed information can be accessed in the Supplementary Data (Supplementary File S5). *circIGHG* expression was then measured using qRT-PCR to divide patients into two groups, High *circIGHG* and Low *circIGHG*, separated by the median level. As such, 64 patients were grouped into High *circIGHG* and Low *circIGHG* group accepted the rest 105 patients because of a dense concentration of identical values at median point, all of which were grouped as Low *circIGHG*. The relationship of *circIGHG* and prognosis of OSCC was determined by Kaplan–Meier analysis, in which it was revealed that stronger *circIGHG* expression was closely correlated with higher

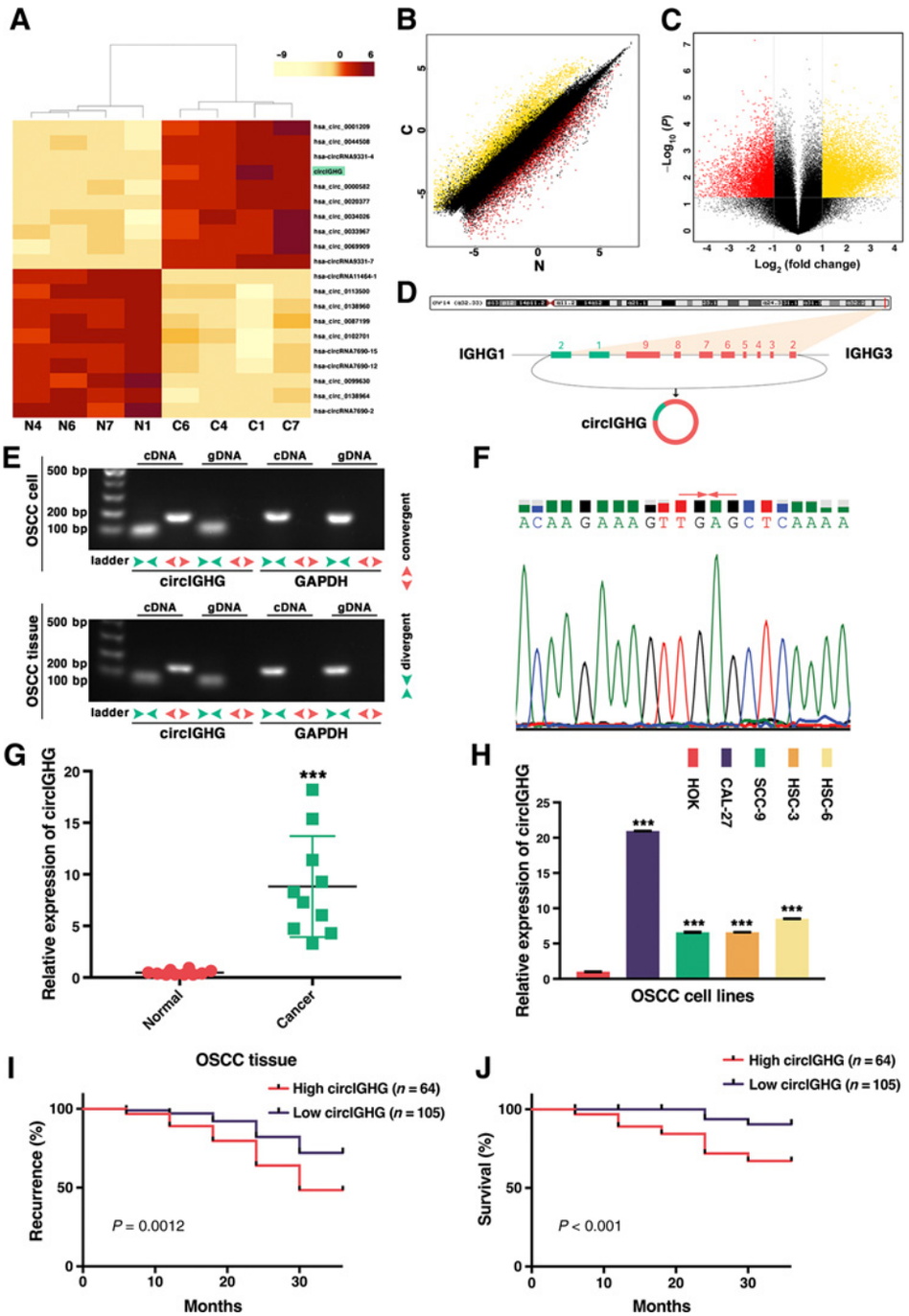

Figure 1.

circIGHG was overexpressed in OSCC. **A,** The top 20 differentially expressed circRNAs in four pairs of human OSCC tissue and matched normal tissue were clustered in a Heatmap matrix. The rows represent OSCC samples (N, normal tissue; C, cancer tissue) and columns represent circRNAs' numerical ID, obtained from circBase. Red, upregulated circRNAs in OSCC; yellow, downregulated circRNAs in OSCC. **B,** Differentially expressed circRNAs between OSCC tissue (yellow dots) and matched normal tissue (red dots) are presented in scatter plot. circRNAs with |fold change| > 2 and $P < 0.05$ are colored. N, normal tissue; C, cancer tissue. **C,** Volcano plot presented significantly differentially expressed circRNAs in OSCC tissue. Upregulated and downregulated circRNAs are plotted in yellow and red color dots, respectively. Threshold was set to $P < 0.05$ and |fold change| > 2. **D,** Schematic illustration showed the genomic loci of *IGHG* gene and *circIGHG*, which was primarily transcribed from a hybrid region of *IGHG1* (exon 1 and 2) and *IGHG3* (exon 2–9). **E,** Agarose gel electrophoresis with RT-PCR products using either divergent and convergent primers in both cDNA and gDNA following RNase R digestion, in both representative OSCC cell line and tissue samples. **F,** Sanger-sequencing result of RT-PCR products amplified with divergent primers. Red arrows, backsplicing junction site. **G** and **H,** Relative expression levels of *circIGHG* in 10 matched pairs of OSCC tissue and normal tissue, as well as in normal HOK and OSCC cell lines. Expression levels were normalized to *GAPDH*. **I** and **J,** Statistical analysis of the correlation of *circIGHG* expression with recurrence and survival in 169 OSCC patients. ***, $P < 0.001$.

frequency of recurrence (**Fig. 1I**), with a recurrence ratio of 51.6% (33/64) found in High *circIGHG* group, compared with a sharply lower portion of 27.6% (29/105) in patients with lower *circIGHG* expression, within 36 months after surgery. Furthermore, overall survival data indicated that *circIGHG* overexpression was also an independent predictor of poor prognosis as High *circIGHG* patients had a significantly worse overall survival than those with lower *circIGHG* levels (**Fig. 1J**). Importantly, Cox regression analysis indicated that the elevated *circIGHG* level was an independent prognostic indicator for patients with OSCC (see Supplementary File S1; Supplementary Table S4). Together, findings from these analyses suggested an important role of *circIGHG* in OSCC progression.

circIGHG directly sponges *miR-142-5p* in OSCC cells

circRNAs are known to behave as endogenous miRNA inhibitors in a sponge-like fashion. Bioinformatic predications (circinteractome.nia.nih.gov; circNet) indicated that *miR-142-5p* was a downstream target of *circIGHG*. To verify the speculation, we first

amplified the predicted binding site with flanking sequences from *circIGHG*. Sanger sequencing of the PCR products verified the existence of complementary *miR-142-5p* base pairing sequences in *circIGHG* (Supplementary File S4). Next, we conducted RNA FISH assay, whose results revealed that *circIGHG* expression possessed a higher adequacy in the OSCC cells than normal oral keratinocytes and was mainly restricted to the cytoplasm (**Fig. 2A**). Furthermore, dual staining of both *circIGHG* and *miR-142-5p* demonstrated their colocalization in OSCC cells, which spatially enabled interaction between them (**Fig. 2B**). qRT-PCR results showed that *miR-142-5p* was sustainably attenuated in response to *circIGHG* mimics treatment in HOK cells, whereas si-*circIGHG* resulted in a considerable upregulation of *miR-142-5p* (**Fig 2C**). However, alterations of *miR-142-5p* did not disturb circIGHG expression (**Fig. 2D**), indicating *miR-142-5p* acting downstream to *circIGHG*. As widely acknowledged, miRNAs function mainly in an RNA-induced silencing complex (RISC)-dependent manner, which requires the participant of a key protein, AGO2. Therefore, it is essential to examine whether *circIGHG* can bind to AGO2. RIP assays were performed in both CAL-27 and HOK cells using AGO2 antibody. The results showed that *circIGHG* was efficiently pulled down by AGO2 antibody with a much greater enrichment in CAL-27 cells than in HOK cells, which indicated that *circIGHG* was specifically enriched by AGO2 antibody (**Fig. 2E**; Supplementary File S3; Supplementary Fig. S4A and S4B). In addition, RNA pull-down assay affirmed the direct binding of *circIGHG* to *miR-142-5p*. Biotin-conjugated *circIGHG* and *miR-142-5p* probes that are complementary to each other were synthesized to enrich *miR-142-5p* and seize *circIGHG*, respectively. As shown in the results, a significant enrichment of *circIGHG* and *miR-142-5p* was seen in **Fig. 2F** and **G**. To further determine the complementarily base-pairing interaction between *circIGHG* and *miR-142-5p*, we mutated the binding site on *circIGHG*. As a result, dual-luciferase reports indicated that with loss of binding site, *circIGHG* failed to sequester *miR-142-5p* (**Fig. 2H**). Those findings supported that *circIGHG* targeted and inhibited *miR-142-5p* activity in a direct binding manner. Furthermore, we quantitively measured the expression of *miR-142-5p* in both OSCC cell lines and tissues against matched normal tissues using qRT-PCR. The results showed that *miR-142-5p* was noticeably downregulated in human OSCC cell lines and cancer tissues ($n = 40$) compared with normal keratinocytes and adjacent normal tissues, respectively (**Fig. 2I–J**), further implying the inhibitory regulation of *circIGHG* on *miR-142-5p*.

IGF2BP3 is a downstream target of *circIGHG*

In attempt to discover the target gene for *circIGHG* signaling, we analyzed two independent assays (GSE3524, GSE31056) from Gene Expression Omnibus (GEO) database (https://www.ncbi.nlm.nih.gov/), both of which strongly indicated that IGF2BP3 was remarkably upregulated in OSCC (GSE3524: fold change = 3.55, $P < 0.05$; GSE31056: fold change = 1.89, $P < 0.001$) versus nontumor tissues (**Fig 3A** and **B**). To validate the data reliance, we measured the protein levels of IGF2BP3 in OSCC in pair with nontumor tissues. It was clearly shown in Western blots and immunofluorescence results that, in agreement with GEO data suggestions, OSCC tissues featured robust IGF2BP3 expression whereas in nontumor tissue, IGF2BP3 was hardly detectable (**Fig. 3C** and **D**). Under closer examination, IGF2BP3 expression was restricted to the cytoplasm of OSCC cells (white arrow, **Fig. 3D**) and had an obviously higher expression along the leading frontiers of the tumor nodules (red arrowhead, **Fig. 3D**), implying its critical role in tumor migration and invasion. Together, protein assay solidified that IGF2BP3 has a significantly elevated activity in OSCC.

Furthermore, to test whether *circIGHG* can manipulate IGF2BP3 via *miR-142-5p*, we designed two siRNA oligos targeting *circIGHG* (si-*circIGHG01*; si-*circIGHG02*). Both were proved capable of functionally annihilating *circIGHG* (**Fig. 2D**). We then treated CAL-27 cells with *circIGHG* mimics and si-*circIGHG* oligos, respectively. Western blot results indicated that while eliminating *circIGHG* led to largely diminished IGF2BP3, addition of *miR-142-5p* inhibitor relieved the reduction of IGF2BP3 (**Fig. 3E**), supporting the previous assumption that *circIGHG* manipulates IGF2BP3 gene activity via *miR-142-5p*. As per bioinformatic analysis, IGF2BP3 has two potential complementary sequences (site-1 and -2) that might serve as anchoring sites for *miR-142-5p*, both of which were then mutated, respectively, to distinguish the exact locus where *miR-142-5p* clings onto (**Fig. 3F**). Following insertion of wild-type and mutated IGF2BP3-3′ UTR sequences into psiCHECK2.0 vectors and cotransfection with *miR-142-5p*, luciferase reports found that mutation at site-1 provoked efficient compensation to the quenched luciferin caused by *miR-142-5p* binding, whereas mutating site-2 induced no notable difference (**Fig. 3G**), indicating that *miR-142-5p* directly binds to IGF2BP3 at site-1.

Silencing *circIGHG* attenuates OSCC aggressiveness

To investigate the role of *circIGHG* in OSCC progression, we silenced *circIGHG* in OSCC cells with lentivirus transfection. Stable depletion of *circIGHG* was tested by qRT-PCR measurement in which the transcription of *circIGHG* was shown to be essentially reduced (Supplementary File S3; Supplementary Fig. S5). To better understand how OSCC cells were influenced following *circIGHG* elimination, we performed a series of experiments to monitor alterations of CAL-27 cells' malignant phenotype, including proliferation, mobility, invasion, and antiapoptosis capability, *in vitro*. To begin with, CCK8 data revealed a remarkably retarded proliferative momentum in both si-*circIGHG* treated groups compared with the vigorous growth in the controls (**Fig. 4A**). Similarly, *circIGHG*-depleted CAL-27 cells were also obviously restrained to heal the scratch (**Fig. 4B**), indicating weakened mobility. Meanwhile, migration and invasion capability of CAL-27 cells were also found to be significantly frustrated by *circIGHG* silencing, suggested by Transwell and Matrigel assays (**Fig. 4C**). In addition, loss of *circIGHG* deprived CAL-27 cells' resistance to CCCP, a chemical that gradually induces death of living cells, as increased caspase-3 expression was detected in si-*circIGHG* groups (**Fig. 4D**). Moreover, *in vivo* experiments in animal models also suggested that si-*circIGHG* contributed significantly to alleviating OSCC cells' tumorigenicity and metastasis through blood vessels (**Fig. 4E–H**). Specifically, immunodeficient nude mice injected with si-*circIGHG*–infected CAL-27 cells developed noticeably smaller xenograft tumors and their lungs also harbored barely none metastatic tumor nodules whereas lungs of mice administrated with vector-treated cells were extensively occupied by metastatic tumors (shown with red arrowheads in **Fig. 4H**), implying that *circIGHG* suppression compromised growth and metastasis of OSCC. Likewise, histologic inspection revealed obviously lower Ki-67 density but higher frequency of round-shaped keratin pearls (shown with green arrowheads in **Fig. 4G**), a structural sign of well differentiation in squamous carcinoma, in si-*circIGHG*–induced xenografts, suggesting milder proliferative impetus and more benign properties in response to *circIGHG* blockage. These findings definitely implied that reduced circIGHG expression substantially weakens aggressiveness of OSCC.

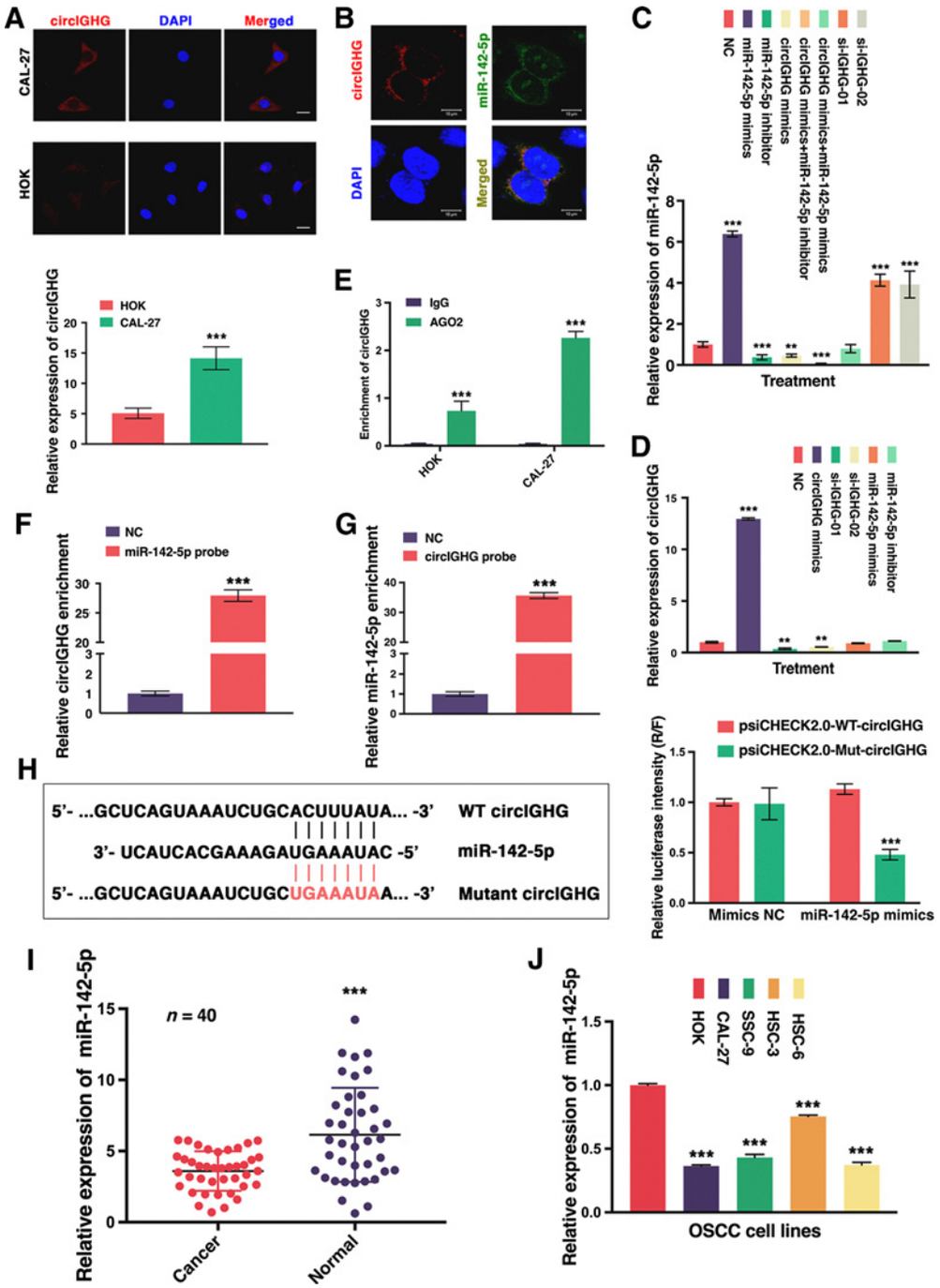

Figure 2.

circIGHG directly sponges *miR-142-5p*. **A,** RNA FISH of *circIGHG* in both HOK and CAL-27 cells. Relative expression levels ware measured by gray value density. Scale bar, 10 μm. **B,** RNA FISH indicated colocalization of *circIGHG* and *miR-142-5p*. Scale bar, 10 μm. **C** and **D,** Expression levels of *circIGHG* and *miR-142-5p* were measured by qRT-PCR. NC, negative control. **E,** Enrichment of *circIGHG* by AGO2 antibody and IgG was assessed by RIP assay in both CAL-27 and HOK cells. **F** and **G,** Expression levels of *circIGHG* and *miR-142-5p* in RNA pull-down products were assessed by qRT-PCR. **H,** Illustration of the wild-type (WT) and mutant (Mut) binding site sequences in *circIGHG* for *miR-142-5p*. Relative luciferase intensity was quantified as ratio of *Renilla* (R) over Firefly (F) luciferase activities. **I** and **J,** Expression levels of *miR-142-5p* in OSCC cancer tissue and cell lines in comparison with matched normal tissue and normal human keratinocytes, respectively, were measured using qRT-PCR. **, $P < 0.01$; ***, $P < 0.001$.

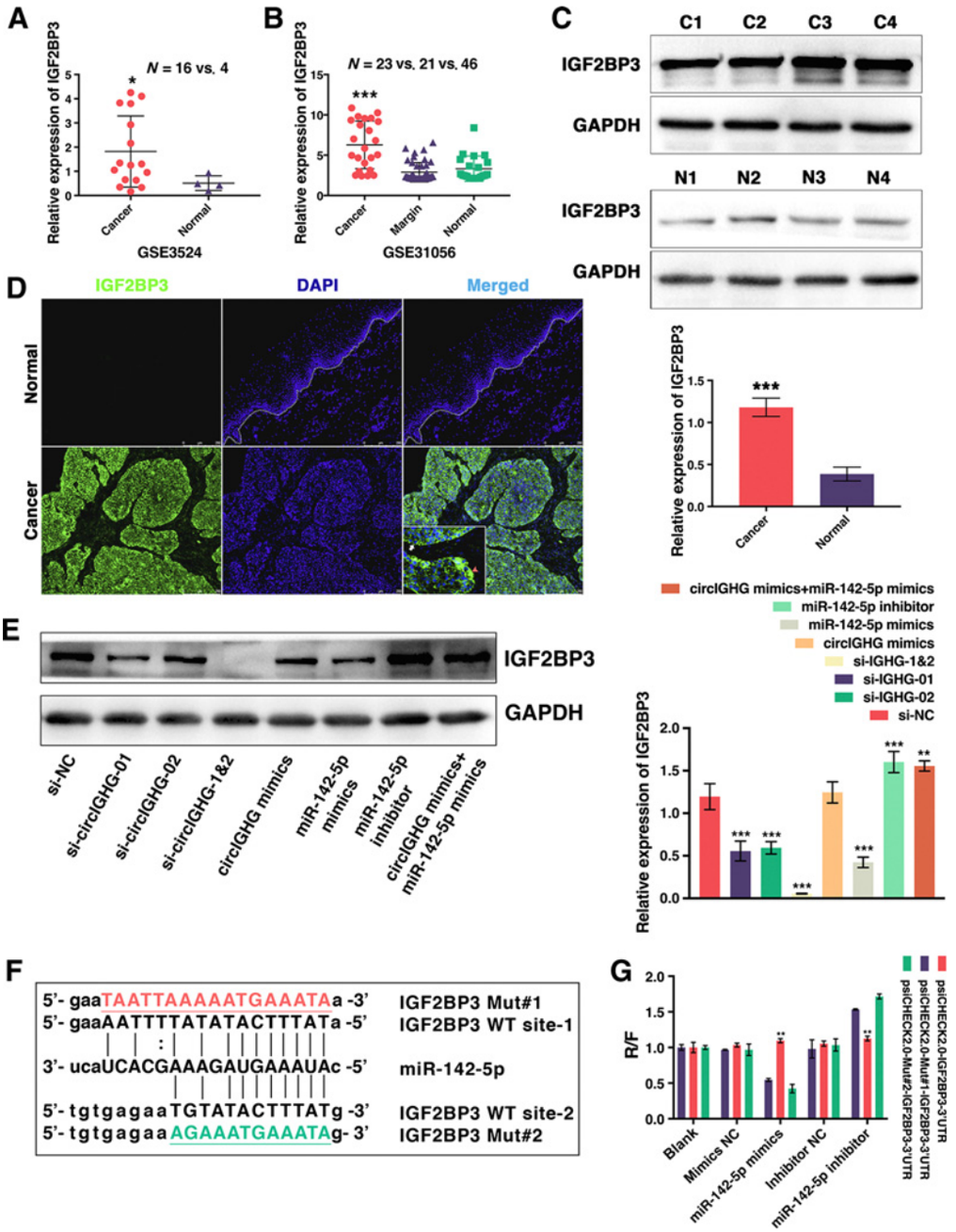

Figure 3.

IGF2BP3 was increased in OSCC and regulated by *circIGHG*. **A** and **B,** Comparison of IGF2BP3 expression levels in OSCC tissues and normal and/or adjacent margin tissue according to the sequencing information retrieved from GEO database (GES3524 and GSE31056). **C,** Western blot analysis compared the expression levels of IGF2BP3 in four paired cancer (C) and normal (N) tissue from patients with OSCC. GADPH served as internal reference. **D,** IF staining showed expression patterns of IGF2BP3 in both OSCC cancer tissue and normal oral mucosa. Dashed line indicates the basement membrane. Inset is a higher magnification. **E,** Changes in IGF2BP3 expression after treatment of mimics or inhibitor of *circIGHG* and *miR-142-5p*, and negative control were measured by Western blot analysis. **F** and **G,** Schematic illustration of the wild-type (WT) and mutant (Mut#1, Mut#2) binding site sequences in IGF2BP3 for *miR-142-5p*. Relative luciferase intensity was quantified as ratio of *Renilla* (R) over Firefly (F) luciferase activities. *, $P < 0.05$; **, $P < 0.01$; ***, $P < 0.001$.

circIGHG induces EMT in OSCC both *in vitro* and *in vivo*

To unveil the underlying mechanism of how *circIGHG* influences OSCC metastasis, we analyzed the expression variations of a bunch of key genes that are critically involved in EMT, a pivotal process that facilitates metastasis in cancer cells (25). Western blots analyses showed that stimulation of *circIGHG* mimics to CAL-27 cells led to more robustly expressed mesenchymal markers, including, SNAI and ZEB2, except that E-cadherin, an epithelial hallmark

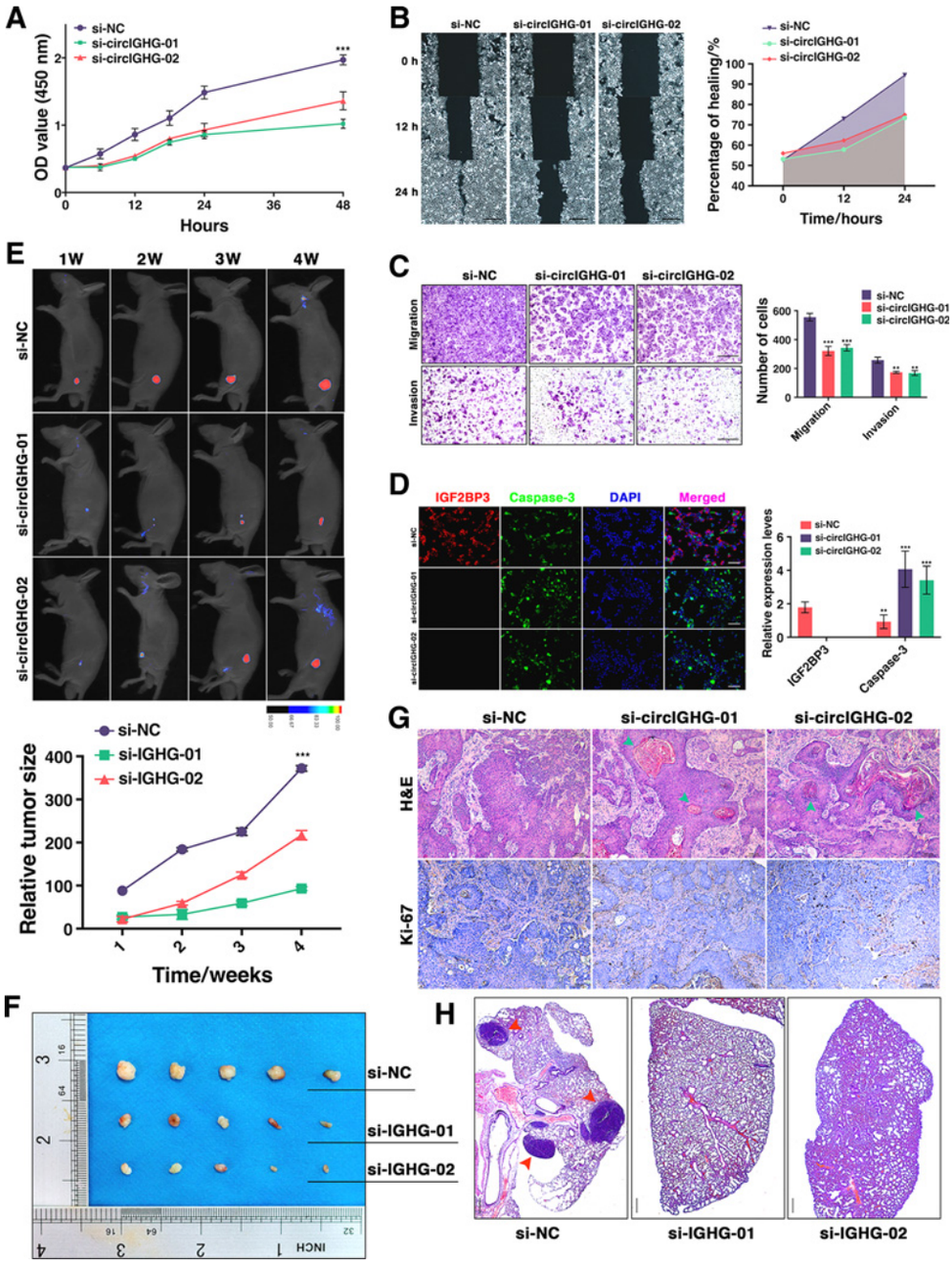

Figure 4.

Knockout of *circIGHG1* impairs aggressiveness of OSCC *in vivo*. **A,** Proliferation of CAL-27 cells with silenced *circIGHG* were examined by CCK8 assays. **B,** Mobility of *circIGHG*-deprived CAL-27 cells were evaluated by wound-healing assay. Scale bar, 300 μm. **C,** Migration and invasion ability of CAL-27 cells after *circIGHG* deletion was assessed in Transwell assay. Scale bar, 300 μm. **D,** Resistance to CCCP-induced apoptosis of CAL-27 cells with absence of *circIGHG* was checked by caspase-3 activity in IF staining. Scale bar, 300 μm. **E** and **F,** Influences of silencing *circIGHG* on tumorigenic capability of CAL-27 cells were evaluated by the volumes of the subcutaneous xenograft tumors in nude mice. **G,** Histologic sections of xenografts were subject to hematoxylin and eosin (H&E) and IHC staining to determine tumor growth and differentiation staging. Scale bar, 100 μm. **H,** Histologic analysis revealed metastatic tumor nodules in lungs of mice injected with CAL-27 cells that were transfected by negative control but not si-*circIGHG*. Scale bar, 500 μm.

was remarkably reduced (**Fig. 5A**). In sharp contrast, silencing *circIGHG* completely reversed the changes (**Fig. 5B**). Next, the xenograft tumors were sectioned to check whether *circIGHG* changes also influenced EMT *in vivo*. Similarly, it was vividly shown in IF staining results that, in consistence with previous findings in cellular experiments, the vector-infected CAL-27–induced tumors possessed strong expression of IGF2BP3 and mesenchymal markers, SNAI and ZEB2, while E-cadherin

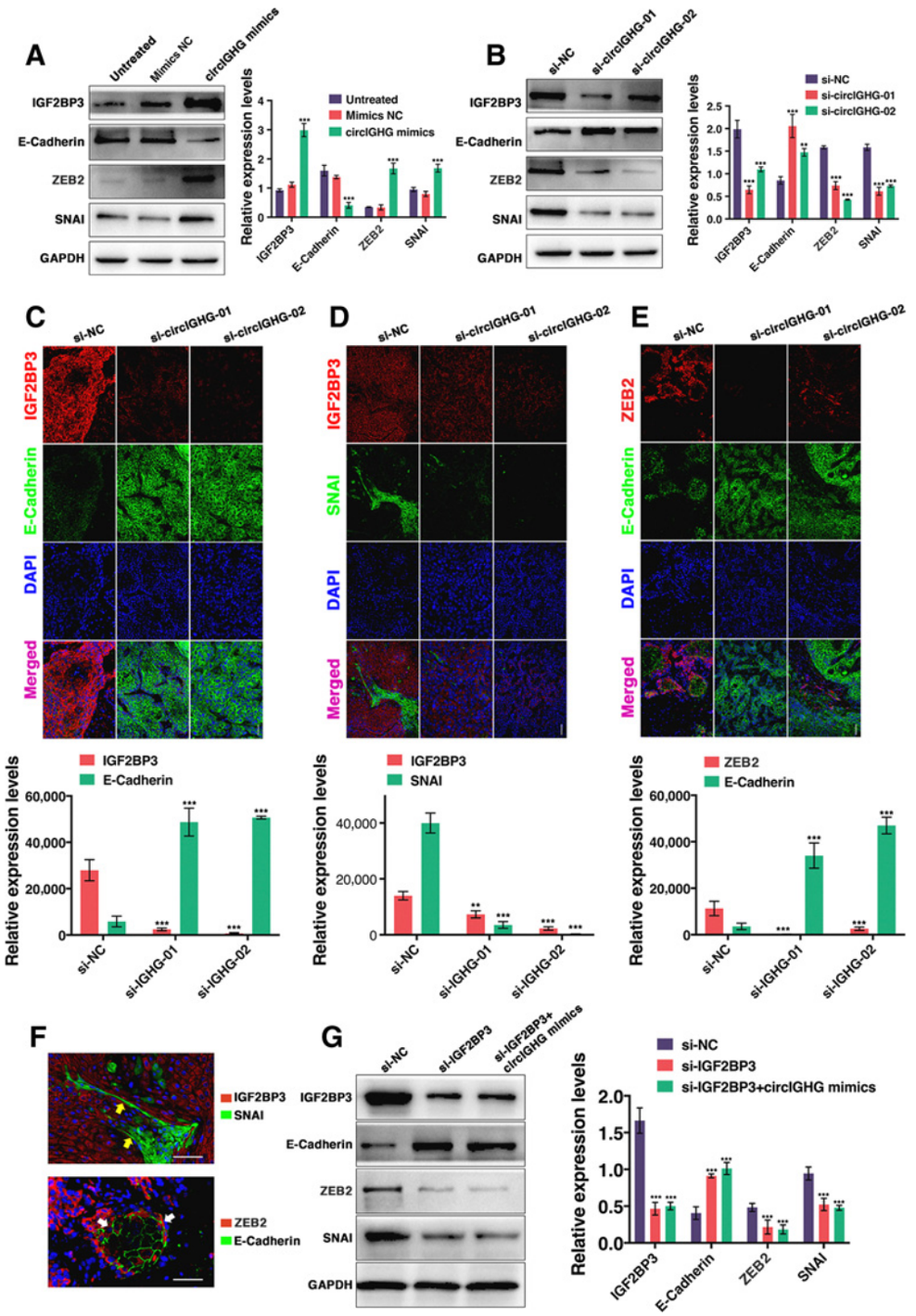

Figure 5.

si-*circIGHG* deactivated EMT in OSCC, both *in vitro* and *in vivo*. **A** and **B,** Western blots showed the changes in expression levels of IGF2BP3, E-cadherin, ZEB2, and SNAI, in response to treatment of *circIGHG* stimulation or elimination, in CAL-27 cells. GAPDH was used as normalization reference. **C**–**E,** Silencing *circIGHG* altered the expression of IGF2BP3, E-cadherin, ZEB2, and SNAI in xenograft tumors, detected by immunofluorescence staining assays. Scale bar, 100 μm. **F,** Higher magnification detailed the morphologic changes in OSCC cells. Scale bar, 50 μm. **G,** Western blotting results showed that blockage of IGF2BP3 via si-IGF2BP3 interference significantly reduced expression of ZEB2 and SNAI but upregulated expression of E-cadherin in CAL-27 cells. Additional stimuli using *circIGHG* mimics to IGF2BP3 knockout did not cause obvious changes in expression of SNAI, E-cadherin, or ZEB2 in CAL-27 cells. GAPDH was used as loading control. **, $P < 0.01$; ***, $P < 0.001$.

expression was fairly faint (**Fig. 5C–E**; Supplementary File S3; Supplementary Fig. S6), indicating actively ongoing EMT. On the other hand, when *circIGHG* was silenced, expression of SNAI and *ZEB2* were both dramatically downregulated, whereas simultaneously, *E-cadherin* gained considerable enhancement (**Fig. 5C–E**). A closer look at the tumors' invading borders further revealed that cancer cells were shedding E-cadherin and acquiring mesenchymal signature proteins (see yellow and white arrows in **Fig. 5F**), implying that cancer cells were genetically undergoing transition from epithelium to mesenchyme. Those findings certainly indicated that *circIGHG* played an essential role in regulating EMT in OSCC.

To verify whether IGF2BP3 is necessary for *circIGHG*-regulating EMT, we then fundamentally knocked out IGF2BP3 using siRNA transfection in CAL-27 cells. Western blots analysis showed that annihilation of IGF2BP3 significantly pulled down SNAI and ZEB2 expression in CAL-27 cells. However, further stimulation by overexpressing *circIGHG* failed to rescue the decline. Similarly, silencing IGF2BP3 remarkably augmented E-cadherin expression in OSCC cells. Yet, addition of *circIGHG* treatment to OSCC cells did not compromise *E-cadherin*'s translation without presence of IGF2BP3 (**Fig. 5G**). Taken together, those observations demonstrated that *circIGHG* promoted metastasis in OSCC via inducing IGF2BP3-mediated EMT.

Discussion

In this study, we revealed a novel mechanism of *circIGHG*-regulating OSCC via *miR-142-5p*/IGF2BP3 pathway (**Fig. 6**). Increasing amount of studies have explored the biogenesis, characters, functions of circular RNAs and demonstrated their aberrant behaviors in a variety of cancers, indicating their potentials in regulating cancer progression (26, 27). Thanks to advance in RNA profiling, floras of circRNAs have been identified in multiple cancers (28–30). To date, nonetheless, rare circRNAs have been associated to OSCC, the most commonly occurring malignancy in head and neck tumors (31, 32). Besides, how circRNAs influence the development and metastasis of OSCC still needs to be further detailed. Presented in this study was a thorough screening of significantly altered circRNAs in OSCC. Functional analysis showed that a significant portion of dysregulated circRNAs have close relationship with cancer development, either by participating in cancer-related biological processes or by exerting specific molecular functions that are critical for carcinogenesis.

Among the varied circRNAs, the plethora of a novel circRNA, *circIGHG*, was confirmed and more importantly, closely correlates with poor prognosis of patients with OSCC. circRNAs function in versatile manners, including but not limited to decoying miRNAs or proteins (33, 34), regulating splicing and transcription (35) and even translating proteins under specific circumstances in certain tissues (36, 37). But currently, it is most maturely established that

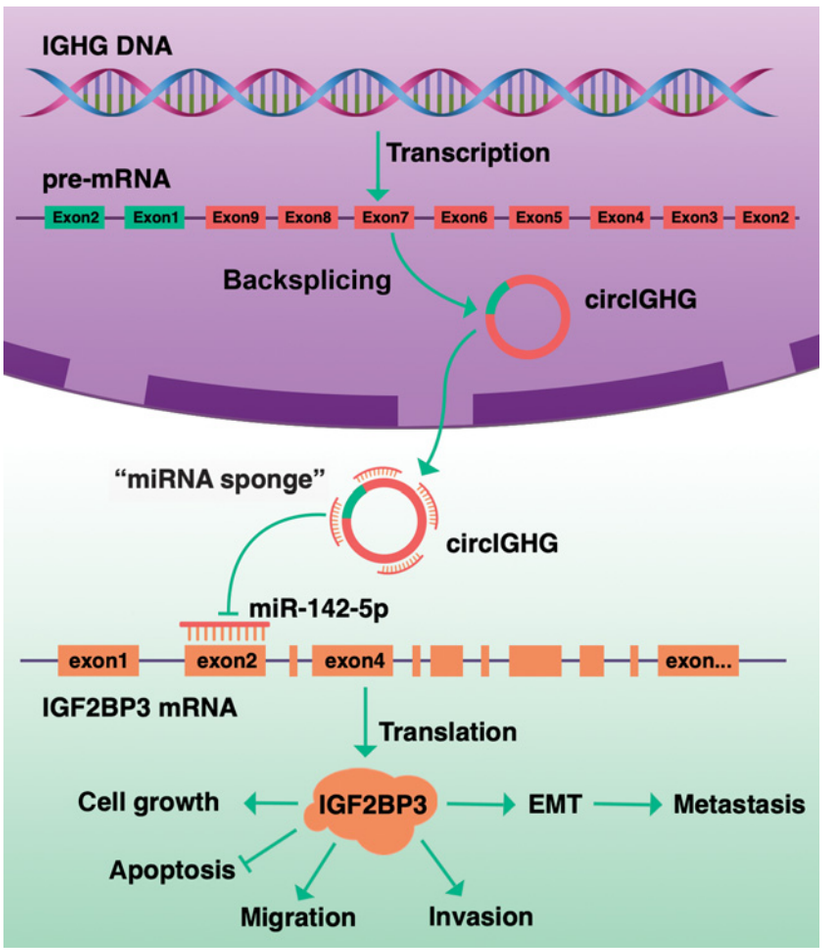

Figure 6.
Schematic graph illustrates the *circIGHG/miR-142-5p*/IGF2BP3 signaling pathway in OSCC. circIGHG promotes IGF2BP3 via sponging *miR-1425-p* and favors growth, invasion, and metastasis of OSCC.

circRNA can effectively recruit and decompose miRNA as they own miRNA-binding sites in high density. Among the candidate miRNA targets, we in this study identified that *miR-142-5p* can be loyally abducted by *circIGHG*. Besides, it is worth to notice that *miR-142-5p* was previously reported as a potential prognostic indicator across types of cancers (38–41). The majority of those reports spontaneously suggested that *miR-142-5p* might possess an antitumor property by hindering cancer growth and high frequency of recurrence and deteriorated survival were expected when *miR-142-5p* was lowered. Our study, in fine agreement with previous findings, also detected profound reduction of *miR-142-5p* in OSCC. Furthermore, we for the first time reported here that *miR-142-5p* can modify IGF2BP3 expression by directly binding to its 3′-UTR. The rigid signaling hierarchy of *circIGHG* sequestering *miR-142-5p*, and thereby stabilizing IGF2BP3 was supported by PCR and luciferase activity assessment performed in this study.

IGF II mRNA-binding protein 3 (IGF2BP3 or IMP3) is an well-known oncofetal mRNA-binding protein, who is mainly actively expressed throughout embryogenesis but barely seen in normal adult organisms (42, 43). Surprisingly, we found that IGF2BP3 was extensively expressed in OSCC tissue and cell lines. And more intriguingly, immunostaining analyses showcased that intensified IGF2BP3 appearance was constantly accompanied by robust EMT marks, such as ZEB2 and SNAI, raising the supposition that if IGF2BP3 contributes to metastasis of OSCC. Cervical lymph node metastasis is an important prognostic marker for OSCC, and lower survival rates were usually associated with patients developing cervical lymph node metastasis (44–46). Therefore, understanding metastasis is a critical step toward prevention. Actually, IGF2BP3 was not for the first time considered a prognostic indicator in OSCC. Numerous studies have indeed suggested that IGF2BP3 promoted invasion and metastasis of OSCC (47–49). Regretfully, however, whether IGF2BP3 induces and tunes EMT was not yet explained. It is well known that EMT is a crucial prerequisite for cancer metastasis though which cancer cells abandon epithelial phenotype and acquire mesenchymal traits, including fibroblast-like morphology and enhanced mobility to invade and metastasize (50). We herein reported that IGF2BP3 essentially participates in inducing EMT and knockout of IGF2BP3 might intercept EMT as E-cadherin, SNAI and ZEB2 failed to respond to *circIGHG* with absence of IGF2BP3, although how IGF2BP3 exquisitely mediates EMT certainly needs to be further elucidated in future research.

In summary, our findings suggested that *circIGHG* obtains augmented expression in OSCC and in consequence, overexpression of *circIGHG* upregulated IGF2BP3 via suppressing *miR-142-5p* and induced EMT, which favors invasion and metastasis of OSCC. Future research on *circIGHG* may provide novel discoveries in OSCC diagnosis and therapy.

Authors' Disclosures

No disclosures were reported.

Authors' Contributions

J. Liu: Conceptualization, data curation, software, formal analysis, funding acquisition, validation, investigation, visualization, methodology, writing-original draft, project administration. **X. Jiang:** Resources, software, formal analysis, investigation. **A. Zou:** Resources, software, investigation, visualization, methodology. **Z. Mai:** Software, validation, investigation. **Z. Huang:** Software, investigation, visualization. **L. Sun:** Software, investigation, visualization. **J. Zhao:** Conceptualization, resources, supervision, funding acquisition, writing-review and editing.

Acknowledgments

This study was funded by the Science Research Cultivation Program of Stomatological Hospital, Southern Medical University (No. PY2018028). The authors thank the staff of the Central Laboratory of Southern Medical University for their generous assistance with confocal and live animal imaging.

The costs of publication of this article were defrayed in part by the payment of page charges. This article must therefore be hereby marked *advertisement* in accordance with 18 U.S.C. Section 1734 solely to indicate this fact.

Received February 17, 2020; revised June 18, 2020; accepted November 12, 2020; published first November 17, 2020.

References

1. Chaturvedi AK, Anderson WF, Lortet-Tieulent J, Curado MP, Ferlay J, Franceschi S, et al. Worldwide trends in incidence rates for oral cavity and oropharyngeal cancers. J Clin Oncol 2013;31:4550–9.
2. Bray F, Ferlay J, Soerjomataram I, Siegel RL, Torre LA, Jemal A. Global cancer statistics 2018: GLOBOCAN estimates of incidence and mortality worldwide for 36 cancers in 185 countries. CA Cancer J Clin 2018;68:394–424.
3. Bhattacharya A, Roy R, Snijders AM, Hamilton G, Paquette J, Tokuyasu T, et al. Two distinct routes to oral cancer differing in genome instability and risk for cervical node metastasis. Clin Cancer Res 2011;17:7024–34.
4. Kim JW, Park Y, Roh J-L, Cho K-J, Choi S-H, Nam SY, et al. Prognostic value of glucosylceramide synthase and P-glycoprotein expression in oral cavity cancer. Int J Clin Oncol 2016;21:883–9.
5. Wu F, Shi X, Zhang R, Tian Y, Wang X, Wei C, et al. Regulation of proliferation and cell cycle by protein regulator of cytokinesis 1 in oral squamous cell carcinoma. Cell Death Dis 2018;9:564.
6. Chen L-L, Yang L. Regulation of circRNA biogenesis. RNA Biol 2015;12:381–8.
7. Wang Y, Wang Z. Efficient backsplicing produces translatable circular mRNAs. RNA 2015;21:172–9.
8. Memczak S, Jens M, Elefsinioti A, Torti F, Krueger J, Rybak A, et al. Circular RNAs are a large class of animal RNAs with regulatory potency. Nature 2013;495:333–8.
9. Thomson DW, Dinger ME. Endogenous microRNA sponges: evidence and controversy. Nat Rev Genet 2016;17:272–83.
10. Kawamata T, Seitz H, Tomari Y. Structural determinants of miRNAs for RISC loading and slicer-independent unwinding. Nat Struct Mol Biol 2009;16:953–60.
11. Sang M, Meng L, Sang Y, Liu S, Ding P, Ju Y, et al. Circular RNA ciRS-7 accelerates ESCC progression through acting as a miR-876-5p sponge to enhance MAGE-A family expression. Cancer Lett 2018;426:37–46.
12. Xue D, Wang H, Chen Y, Shen D, Lu J, Wang M, et al. Circ-AKT3 inhibits clear cell renal cell carcinoma metastasis via altering miR-296-3p/E-cadherin signals. Mol Cancer 2019;18:151.
13. Zhang P-F, Pei X, Li K-S, Jin L-N, Wang F, Wu J, et al. Circular RNA circFGFR1 promotes progression and anti-PD-1 resistance by sponging miR-381-3p in non-small cell lung cancer cells. Mol Cancer 2019;18:179.
14. Chen F, Qi S, Zhang X, Wu J, Yang X, Wang R. miR-23a-3p suppresses cell proliferation in oral squamous cell carcinomas by targeting FGF2 and correlates with a better prognosis: miR-23a-3p inhibits OSCC growth by targeting FGF2. Pathol Res Pract 2019;215:660–7.
15. Wang Y, Zhang X, Wang Z, Hu Q, Wu J, Li Y, et al. LncRNA-p23154 promotes the invasion-metastasis potential of oral squamous cell carcinoma by regulating Glut1-mediated glycolysis. Cancer Lett 2018;434:172–83.
16. McBride OW, Battey J, Hollis GF, Swan DC, Siebenlist U, Leder P. Localization of human variable and constant region immunoglobulin heavy chain genes on subtelomeric band q32 of chromosome 14. Nucleic Acids Res 1982;10:8155–70.
17. Croce CM, Shander M, Martinis J, Cicurel L, D'Ancona GG, Dolby TW, et al. Chromosomal location of the genes for human immunoglobulin heavy chains. Proc Natl Acad Sci U S A 1979;76:3416–9.
18. Pandey JP, Nietert PJ, Klaamas K, Kurtenkov O. A genetic variant of immunoglobulin γ2 is strongly associated with immunity to mucin 1 in patients with breast cancer. Cancer Immunol Immunother 2009;58:2025–9.

19. Pandey J, Namboodiri A, Ohue Y, Oka M, Nakayama E. Genetic variants of immunoglobulin γ and κ chains influence humoral immunity to the cancer-testis antigen XAGE-1b (GAGED 2a) in patients with non-small cell lung cancer. Clin Exp Immunol 2014;176:78–83.
20. Chu J, Li Y, Deng Z, Zhang Z, Xie Q, Zhang H, et al. IGHG1 regulates prostate cancer growth via the MEK/ERK/c-Myc pathway. Biomed Res Int 2019;2019; 7201562.
21. Lal A, Thomas MP, Altschuler G, Navarro F, O'Day E, Li XL, et al. Capture of microRNA–bound mRNAs identifies the tumor suppressor miR-34a as a regulator of growth factor signaling. PLos Genet 2011;7:e1002363.
22. Liu J, Chanumolu S, Krei Z, Albahrani M, Akhtam A, Jia Z, et al. Identification of genes differentially expressed in simvastatin-induced alveolar bone formation. JBMR Plus 2019;3:e10122.
23. Liu X, Abraham JM, Cheng Y, Wang Z, Wang Z, Zhang G, et al. Synthetic circular RNA functions as a mir-21 sponge to suppress gastric carcinoma cell proliferation. Mol Ther Nucleic Acids 2018;13:312–21.
24. Hu L, Liu J, Li Z, Ozturk F, Gurumurthy C, Romano RA, et al. TGFβ3 regulates periderm removal through ΔNp63 in the developing palate. J Cell Physiol 2015; 230:1212–25.
25. Brabletz T, Kalluri R, Nieto MA, Weinberg RA. EMT in cancer. Nat Rev Cancer 2018;18:128–34.
26. Qian L, Yu S, Chen Z, Meng Z, Huang S, Wang P. The emerging role of circRNAs and their clinical significance in human cancers. Biochim Biophys Acta Rev Cancer 2018;1870:247–60.
27. Kristensen L, Hansen T, Venø M, Kjems J. Circular RNAs in cancer: opportunities and challenges in the field. Oncogene 2018;37:555–65.
28. Peng L, Yuan XQ, Li GC. The emerging landscape of circular RNA ciRS-7 in cancer. Oncol Rep 2015;33:2669–74.
29. Su M, Xiao Y, Ma J, Tang Y, Tian B, Zhang Y, et al. Circular RNAs in cancer: emerging functions in hallmarks, stemness, resistance and roles as potential biomarkers. Mol Cancer 2019;18:90.
30. Bach D-H, Lee SK, Sood AK. Circular RNAs in cancer. Mol Ther Nucleic Acids 2019;16:118–29.
31. Guo Y, Yang J, Huang Q, Hsueh C, Zheng J, Wu C, et al. Circular RNAs and their roles in head and neck cancers. Mol Cancer 2019;18:44.
32. Momen-Heravi F, Bala S. Emerging role of non-coding RNA in oral cancer. Cell Signal 2018;42:134–43.
33. Kulcheski FR, Christoff AP, Margis R. Circular RNAs are miRNA sponges and can be used as a new class of biomarker. J Biotechnol 2016;238:42–51.
34. Hansen TB, Jensen TI, Clausen BH, Bramsen JB, Finsen B, Damgaard CK, et al. Natural RNA circles function as efficient microRNA sponges. Nature 2013;495: 384–8.
35. Li Z, Huang C, Bao C, Chen L, Lin M, Wang X, et al. Exon-intron circular RNAs regulate transcription in the nucleus. Nat Struct Mol Biol 2015;22:256–64.
36. Pamudurti NR, Bartok O, Jens M, Ashwal-Fluss R, Stottmeister C, Ruhe L, et al. Translation of circRNAs. Mol Cell 2017;66:9–21.
37. Yang Y, Fan X, Mao M, Song X, Wu P, Zhang Y, et al. Extensive translation of circular RNAs driven by N 6-methyladenosine. Cell Res 2017;27:626–41.
38. Zhang X, Yan Z, Zhang J, Gong L, Li W, Cui J, et al. Combination of hsa-miR-375 and hsa-miR-142-5p as a predictor for recurrence risk in gastric cancer patients following surgical resection. Ann Oncol 2011;22:2257–66.
39. Jia L, Xi Q, Wang H, Zhang Z, Liu H, Cheng Y, et al. miR-142-5p regulates tumor cell PD-L1 expression and enhances anti-tumor immunity. Biochem Biophys Res Commun 2017;488:425–31.
40. Wang Z, Liu Z, Fang X, Yang H. MiR-142-5p suppresses tumorigenesis by targeting PIK3CA in non-small cell lung cancer. Cell Physiol Biochem 2017;43:2505–15.
41. Islam F, Gopalan V, Vider J, Lu C-t, Lam AK-Y. MiR-142-5p act as an oncogenic microRNA in colorectal cancer: clinicopathological and functional insights. Exp Mol Pathol 2018;104:98–107.
42. Nielsen J, Christiansen J, Lykke-Andersen J, Johnsen AH, Wewer UM, Nielsen FC. A family of insulin-like growth factor II mRNA-binding proteins represses translation in late development. Mol Cell Biol 1999;19:1262–70.
43. Mueller-Pillasch F, Pohl B, Wilda M, Lacher U, Beil M, Wallrapp C, et al. Expression of the highly conserved RNA binding protein KOC in embryogenesis. Mech Dev 1999;88:95–9.
44. Ferlito A, Rinaldo A, Devaney KO, MacLennan K, Myers JN, Petruzzelli GJ, et al. Prognostic significance of microscopic and macroscopic extracapsular spread from metastatic tumor in the cervical lymph nodes. Oral Oncol 2002; 38:747–51.
45. Mamelle G, Pampurik J, Luboinski B, Lancar R, Lusinchi A, Bosq J. Lymph node prognostic factors in head and neck squamous cell carcinomas. Am J Surg 1994; 168:494–8.
46. Liao C-T, Hsueh C, Lee L-Y, Lin C-Y, Fan K-H, Wang H-M, et al. Neck dissection field and lymph node density predict prognosis in patients with oral cavity cancer and pathological node metastases treated with adjuvant therapy. Oral Oncol 2012;48:329–36.
47. Li H-G, Han J-J, Huang Z-Q, Wang L, Chen W-L, Shen X-M. IMP3 is a novel biomarker to predict metastasis and prognosis of tongue squamous cell carcinoma. J Craniofac Surg 2011;22:2022–5.
48. Li S, Cha J, Kim J, Kim KY, Kim HJ, Nam W, et al. Insulin-like growth factor II mRNA-binding protein 3: a novel prognostic biomarker for oral squamous cell carcinoma. Head Neck 2011;33:368–74.
49. Lin CY, Chen ST, Jeng YM, Yeh CC, Chou HY, Deng YT, et al. Insulin-like growth factor II mRNA-binding protein 3 expression promotes tumor formation and invasion and predicts poor prognosis in oral squamous cell carcinoma. J Oral Pathol Med 2011;40:699–705.
50. Yang J, Weinberg RA. Epithelial-mesenchymal transition: at the crossroads of development and tumor metastasis. Dev Cell 2008;14:818–29.